Global Spatial Normalization of Human Brain Using Convex Hulls

Jack L. Lancaster, Peter T. Fox, Hunter Downs, Daniel S. Nickerson, Trish A. Hander, Mohammed El Mallah, Peter V. Kochunov and Frank Zamarripa

Departments of Radiology, Medicine, Psychiatry and Psychology and Research Imaging Center, University of Texas Health Sciences Center at San Antonio, Texas; and Department of Neurological Surgery, Radiology and Biomedical Engineering, Virginia Neurological Institute, University of Virginia, Charlottesville, Virginia

Global spatial normalization transforms a brain image so that its principal global spatial features (position, orientation and dimensions) match those of a standard or atlas brain, supporting consistent analysis and referencing of brain locations. The convex hull (CH), derived from the brain's surface, was selected as the basis for automating and standardizing global spatial normalization. The accuracy and precision of CH global spatial normalization of PET and MR brain images were evaluated in normal human subjects. **Methods:** Software was developed to extract CHs of brain surfaces from tomographic brain images. Pelizzari's hat-to-head least-square-error surface-fitting method was modified to fit individual CHs (hats) to a template CH (head) and calculate a nine-parameter coordinate transformation to perform spatial normalization. A template CH was refined using MR images from 12 subjects to optimize global spatial feature conformance to the 1988 *Talairach Atlas* brain. The template was tested in 12 additional subjects. Three major performance characteristics were evaluated: (a) quality of spatial normalization with anatomical MR images, (b) optimal threshold for PET and (c) quality of spatial normalization for functional PET images. **Results:** As a surface model of the human brain, the CH was shown to be highly consistent across subjects and imaging modalities. In MR images (n = 24), mean errors for anterior and posterior commissures generally were <1 mm, with SDs < 1.5 mm. Mean brain-dimension errors generally were <1.3 mm, and bounding limits were within 1–2 mm of the *Talairach Atlas* values. The optimal threshold for defining brain boundaries in both ^{18}F-fluorodeoxyglucose (n = 8) and ^{15}O-water (n = 12) PET images was 40% of the brain maximum value. The accuracy of global spatial normalization of PET images was shown to be similar to that of MR images. **Conclusion:** The global features of CH-spatially normalized brain images (position, orientation and size) were consistently transformed to match the *Talairach Atlas* in both MR and PET images. The CH method supports intermodality and intersubject global spatial normalization of tomographic brain images.

Key Words: convex hull; *Talairach Atlas*; global spatial normalization; regional spatial normalization

J Nucl Med 1999; 40:942–955

The ultimate goal of brain spatial normalization is to transform brain image volumes to a standard atlas brain so that corresponding structures coincide spatially. Numerous algorithms have been proposed for spatial normalization, ranging from global affine transformations (*1–5*) to regional deformations (*6–10*). Talairach global spatial normalization seeks to adjust brain image data to conform to the principal defining global features of Talairach and Tournoux's 1988 *Co-Planar Stereotaxic Atlas of the Brain (Talairach Atlas)* (*11*) brain space (brain origin, orientation and dimensions). Regional methods attempt to extend spatial normalization to the smallest resolved structures. Global spatial normalization has been shown to enhance detection of focal brain response in PET studies when intersubject averaging is used (*8,12,13*). *Talairach Atlas* coordinates from globally spatially normalized images are commonly used for reporting research findings (*14*) and for recording their locations in databases such as BrainMap (*15*). Even results of brain studies using regional spatial normalization are reported using Talairach coordinates (*12,16*).

In 1990, Bloch (*17*) proposed the use of the convex hull (CH) for feature matching with a biological application in three-dimensional pattern recognition of molecule structure. Bloch later collaborated with Mangin et al. (*18*) to develop a method for registration of PET and MR images of the brain, but the CH was not used. In 1994, Downs et al. (*6*) introduced the CH as a surface-based model for regional spatial normalization. A regional radial-warping method was developed to scale brain images using the anterior commissure (AC) as a fixed internal reference point and the CH as the reference surface for matching. The objective was to reduce intersubject spatial variability in ^{15}O-water cerebral blood flow (CBF) PET images to improve group statistical parametric images (SPIs) (*12,13*) while maintaining a consistent reference to the stereotactic space defined by Talairach and Tournoux (*11*). Early findings were promising but inconclusive as to whether the radial-scaling CH method was better than alternative high-degree-of-freedom methods for regional spatial normalization (*7*). Current research is focused on the improvement and evaluation of the global

spatial normalization component of the original regional CH algorithm.

The CH method resolves several problems often encountered during spatial normalization of low-resolution functional PET and SPECT images. The CH method does not require an MR image because it is based on a single, highly refined template. Also, the CH method works well with limited z-axis extent imagers, supporting its use with older PET images. These combined features support analysis of functional brain images that otherwise might not be possible with other spatial normalization methods.

CONVEX-HULL THEORY

A CH of a set of points is the smallest convex set containing the points (19). A two-dimensional illustration of a CH of the brain is provided in the axial-section images of Figure 1. The CH has several intrinsic properties that make it an attractive model for automated global spatial normalization of the brain. First, the brain surface has both convex (gyral) and concave (sulcal) regions, although most of the anatomic variability is associated with concave regions (20). The CH of a brain is a mathematical representation of the surface that tends to retain gyral and discard sulcal regions. The discarded regions (principally sulci) are replaced with convex equivalents spanning the concavities (Fig. 1), resulting in a brain-surface model with reduced anatomic variability. Second, the brain surface is difficult to resolve accurately and consistently in tomographic images because of regional variations in partial-volume averaging. Although partial-volume averaging is similar over most of the brain's convex surface (gyral regions), there is a high degree of variability in partial-volume effects within convoluted sulcal regions. Therefore, convex brain-surface regions are simpler to consistently resolve and extract, and the CH can be more accurately synthesized than the full brain surface. This leads to a more accurate and reproducible representation of the CH within and across subjects and modalities. Third, the
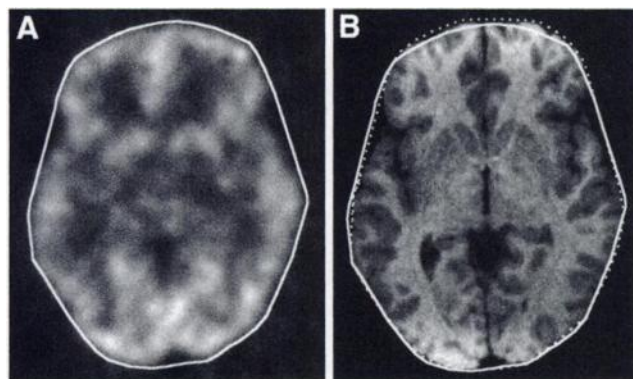

FIGURE 1. CH contours in axial-section images of same subject. (A) [18]FDG PET study with CH (solid outline) determined by 40% threshold. (B) Three-dimensional, gradient-echo, T1-weighted MR image at same section location. CHs derived from MR (broken outline) and [18]FDG PET images demonstrate their similarity in these imaging modalities.

brain is sufficiently complex in shape to support unique alignment using only its surface features (18,21,22). The CH retains critical surface features needed to accurately represent dimension (a surface feature) and orientation (three-dimensional shape asymmetry) (Fig. 2). Finally, the CH was found to exhibit a consistent relationship with internal landmarks (AC and posterior commissure [PC]). These intrinsic properties suggest that the CH will be an effective model for use in global spatial normalization. The central hypothesis is that when CHs are used for global spatial normalization, transformed brains will be highly consistent in dimension, orientation and position and will conform to these features of the *Talairach Atlas* brain.

MATERIALS AND METHODS

Scan and Study Information

High-resolution, T1-weighted, three-dimensional MR, ^{15}O-water CBF and ^{18}F-fluorodeoxyglucose (FDG) images from healthy subjects were analyzed retrospectively to evaluate CH global spatial normalization.

Three-Dimensional MRI (Group 1). Group 1 consisted of 7 men and 5 women (age range 19–48 y, mean age 30.2 ± 10.2 y). MR images were acquired using three-dimensional, T1-weighted, gradient-echo pulse sequences on a 1.9-T Elscint Prestige imager (Markham, Haifa, Israel). Slice spacing ranged from 1.2 to 2.0 mm, and pixel spacing generally was <1 mm. Because this was a retrospective study, pulse-sequence parameters, spacing and orientation were not strictly controlled. Eight of the MR images were acquired as axial sections, and four were acquired as coronal sections. Although it was not the goal of this investigation to evaluate spatial normalization under various imaging conditions, the variety served to illustrate the nature of the spatial normalization methods tested. All MR images were evaluated visually on axial, sagittal and coronal views and judged to be of high quality and well suited for extracting reference brain surfaces for the CH evaluation.

Three-Dimensional MRI (Group 2). Group 2 consisted of 11 men and 1 woman (age range 23–55 y, mean age 31.2 ± 9.6 y). Members of this group were selected from two PET studies and were well matched with the members of group 1. MR images of group 2 were acquired in a manner similar to those of group 1. Nine of the MR images were acquired as axial sections, and three were acquired as sagittal sections. Nine male members of group 2 were from the same PET study, and these subjects were used for the PET analyses.

PET Images. All images were acquired on a GE/Scanditronix model 4096 camera (General Electric, Uppsala, Sweden) with pixel spacing of 2.6 mm; specified spatial resolution of 6 mm full width at half maximum (FWHM); interplane, center-to-center distance of 6.5 mm; 15 scan planes; and z-axis field of view (FOV) ~100 mm. Attenuation correction was performed with a [68]Ge/^{68}Ga pin source. All PET images were reconstructed in a 128 × 128 matrix using 2-mm spacing (256-mm x- and y-axes FOV). Reconstructed image resolution, including all filtering, is estimated to be 7–8 mm FWHM.

[15]O-Water. CBF data were collected during a 90-s scanning period after intravenous injection of ^{15}O-water. The scan was triggered as the tracer bolus entered the FOV (the brain) by the rise in the coincidence counting rate. Sixty milliCuries (2220 MBq)
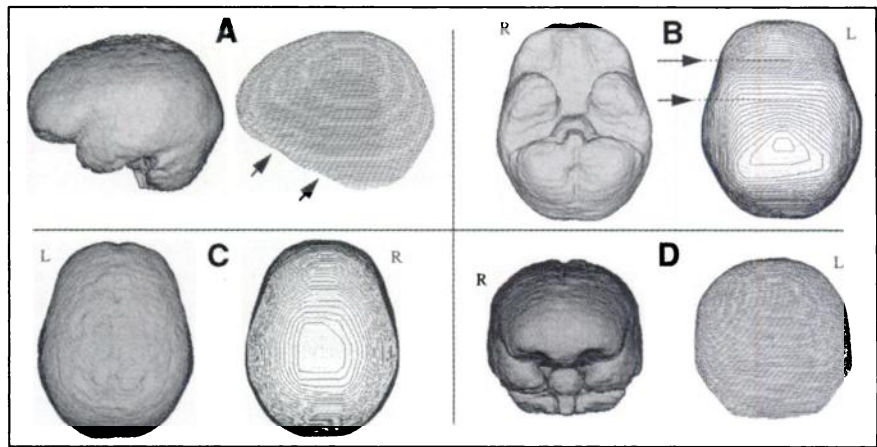
FIGURE 2. Three-dimensional surface view of composite MR image (left) used to synthesize template CH (right) for left lateral (A), inferior (B), superior (C) and anterior views (D). Note highly convex nature of template for most of brain surface and slight departure from convexity (arrows) along inferior boundary.

^{15}O-water (half-life = 123 s) were administered as an intravenous bolus of 8–10 mL saline. A 10-min interscan interval was sufficient for isotope decay (five physical half-lives). Brain blood flow was assumed to be proportional to pixel values.

^{18}F-FDG. Regional cerebral glucose metabolism was measured in patients and controls using ^{18}F-FDG and PET. All subjects were scanned under identical conditions: supine, awake and resting with eyes closed and ears uncovered. A 185-MBq (5-mCi) dose of FDG was injected intravenously, and image acquisition began 40 min after injection. Absolute glucose utilization rate was not measured.

PET Analysis

PET ^{15}O-water functional activation images were analyzed to determine sites of brain activation in a paired-subtraction study. Images from 9 of the 12 group 2 subjects, taken from a previously analyzed study, were reanalyzed. This analysis was done using inhouse software (MIPS; http://ric.uthscsa.edu/projects/mips). All images were transformed into Talairach space (2-mm isometric spacing) using the CH method. A processing mask was used to isolate brain from nonbrain regions of the image, and brain pixel values were scaled to produce a mean value of 1000 within the masked region. Average images for two task states (three repetitions of chorus reading, three repetitions of eyes-closed rest) were calculated for each subject. Average images were subtracted to form a chorus-minus-rest image for each subject. A z-score SPI was calculated for each subject by dividing each pixel in the chorus-minus-rest image by the SD within the brain mask. The spatially normalized SPI was analyzed using change-distribution analysis (*12*) to determine x, y and z Talairach coordinates of activation sites using a local-extremum centroid method.

Brain Convex-Hull Software

The design and development of software for automated implementation of global spatial normalization using the CH method is complete. Earlier work with the regional CH method (*7*) led to software tools to extract CHs from three-dimensional brain images and to create a *Talairach Atlas* template CH. The CH software was refined to improve speed and better manage problems with brain and array boundaries. CH synthesis is based on three orthogonal applications of Melkman's (*23*) two-dimensional polyline CH algorithm. The surface-fitting software developed by Pelizzari et al. (*21*) was used as the means to analyze feature differences between subject and template CHs and to calculate six-parameter (rigid body) or nine-parameter (global) transformations that minimized the mean square error (MSE) between the surfaces. The Pelizzari

software was carefully integrated into the CH software by replacing its head (contour) and hat (point) data structures with head and hat CH equivalents. The final software was further enhanced to enable processing of images in a standard orientation using world coordinates measured in millimeters regardless of the source image orientation, pixel spacing or slice spacing. A stand-alone Xwindows-based UNIX application (Sun Solaris 2.x; Sun Microsystems, Palo Alto, CA) with a convenient user interface completed the development. The resulting "chsn" software was used for the controlled study of the capabilities of CH global spatial normalization.

Global brain image differences develop from extrinsic sources such as imaging technique (position and orientation) and intrinsic sources such as variations in brain dimensions. A nine-parameter global affine transformation was used in the "chsn" software because its nine parameters (three each for translation, rotation and scaling) can be independently optimized to match the principal global features of a test CH to those of the template CH. Three additional global affine parameters, a symmetric shear term for each axis, are possible for three-dimensional images, but shear is not a primary global feature of the brain's CH.

Talairach Atlas Template Convex Hull

The original 1988 *Talairach Atlas* CH template was extracted from MR brain images in seven healthy subjects, each independently spatially normalized. These images were used to form a composite in which the degree of overlap was indicated by pixel value. Using this composite brain image, a template CH was formed that consistently followed the brain surface in at least four of the seven subjects. This template was evaluated previously in 16 subjects using the regional CH method (*7*). However, it was never refined to optimally conform to the global features of the 1988 *Talairach Atlas* brain. A new template was created from the original composite brain image with several modifications. It was shifted to match the AC location of the inhouse standard used for analysis (see Template Convex-Hull Refinement section). Trilinear interpolation used for this transformation resulted in slight smoothing of the image. A threshold of 80% of the maximum pixel value was determined to be optimal for extracting a CH that best matched the original template. The CH is hypothesized to have a high degree of anatomic consistency across subjects, and the seven brains used for synthesis of the *Talairach Atlas* template CH are believed to be sufficient for template development. The composite MR image and template CH are illustrated in Figure 2.

Template Convex-Hull Refinement

MR images were acquired as for group 1. Residual orientation, size and position errors relative to the 1988 *Talairach Atlas* after CH global spatial normalization were used to adjust the composite brain image from which the template CH was synthesized. Special utilities within the spatial normalization software were used to manually perform rotation, scaling and translation and to reslice the transformed images (*5*). This was done in an iterative manner. First, AC–PC line orientation differences about the x- and z-axes were estimated. Orientation about the y-axis was not changed because visual inspection of the midsagittal plane indicated no change was needed. Additionally, y-axis orientation was verified using the midsagittal plane during template development (*7*). Residual orientation errors, mainly about the x-axis, were removed by reorienting the composite brain, and an intermediate CH template was synthesized from the composite. The 12 MR images in group 1 were again CH globally spatially normalized using the oriented intermediate CH template. Major dimensions were measured, and scale factors were calculated to match mean brain dimensions to those of the *Talairach Atlas*. These were applied to the composite brain image, and an oriented and scaled intermediate CH template was synthesized. The 12 group 1 images were again globally spatially normalized using this intermediate template. The difference between the mean location of the AC and its targeted location relative to the image edges (128 mm from left, 107 mm from anterior and 88 mm from superior) was calculated. The composite brain image was translated and a final refined template synthesized. All subsequent testing and use of the CH method were performed with this refined CH template.

An independent estimate of the transformation parameters used in the refinement process was made by fitting the CH from the original composite image (before any adjustments) to the final CH template and comparing rotation and scaling parameters for fit. The targeted and measured rotation and scaling parameters were within 0.1° for rotation and 0.007 for scaling.

Spatial Normalization

Anatomic Images—Group 1. All group 1 MR images were spatially normalized using the CH method and a previously validated manual spatial normalization method (*5*). MRI-derived CHs for each subject were created using images manually edited to remove nonbrain structures. Editing included removal of the brain stem below the level of the inferior margin of the cerebellum. A threshold value (1% of the brain maximum pixel value) was used to extract the brain surface and synthesize its CH. The group 1 CH-transformed MR images were evaluated by comparing landmarks and features to those of the 1988 *Talairach Atlas*. The locations of the AC, PC and brain-"bounding-box" limits were recorded for CH- and manually spatially normalized images. The AC and PC were located using axial and sagittal views of MR images of all subjects. A cursor was used to record x, y and z coordinates in millimeters of the centers of the AC and PC. Additionally, the anterior, posterior, left, right, superior and inferior brain-bounding-box limits were recorded. The inferior limit of the temporal lobe was used as the inferior brain margin in accordance with the *Talairach Atlas*. The brain-bounding-box limit was designated by using the first slice (1-mm spacing) containing brain tissue when viewed in an appropriate section image. The anterior-posterior, left-right (LR) and superior-inferior dimensions of the brain were calculated from these measurements. Orientation errors of the AC–PC line for rotations about the x- and z-axes were calculated using individual AC and PC measurements. Errors for rotation about the y- and z-axes of the midsagittal plane also were estimated by visual inspection in sagittal and axial sections using the spatial normalization software (*5*).

Anatomic Images—Group 2. The goal of this testing was to measure the performance of the refined CH template in a group of subjects not used in the CH template refinement. MR images from 12 additional subjects were evaluated as for group 1. An additional test was performed using nine PET images from each of 9 subjects in this group. The repeat scans were used to estimate the reproducibility of each of the nine parameters used for CH global spatial normalization. A pooled variance across all subjects was calculated for each parameter. The assumption was no head movement for repeat scans. Although this is not possible, even with custom-molded head restraints, these measures provided operational estimates of transformation parameter reproducibility.

Rotational Characteristics

Two measurements were made to study the rotational characteristics of the CH and the CH-fitting method: (a) the MSE between unrotated and rotated CHs and (b) the residual MSE after reorientation to an unrotated standard using the CH method. These measurements were taken from the 12 group 2 MR images. MR images were used because their CHs cover the full brain (Fig. 3). An unrotated image for each subject was standardized using a
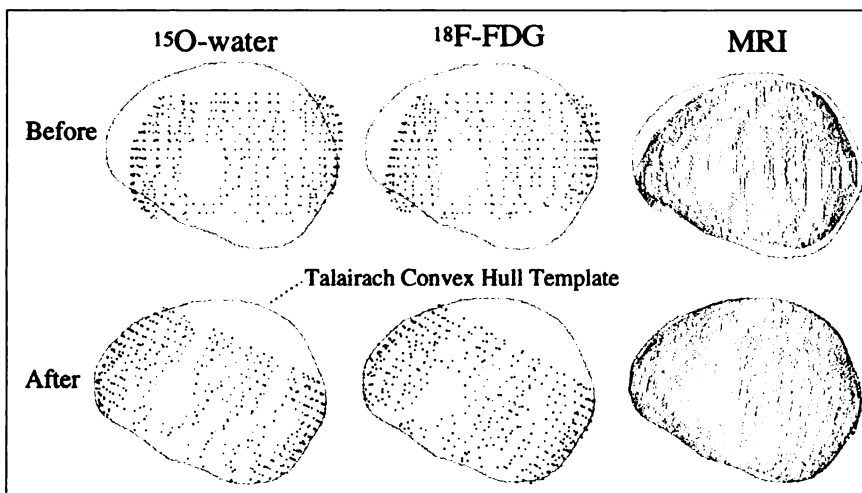

FIGURE 3. Left lateral views of CHs before and after fitting to CH template for 15O-water PET, FDG PET and T1-weighted three-dimensional MR images of same subject. Lighter points are on far side. Silhouette outlining CH template is provided for comparison. Residual RMS error for fitting was <1.5 mm for all three image types.

two-step process. First, it was oriented to the *Talairach Atlas* standard using the CH method. It was then translated so that a midbrain site (midthalamus) would be at the center of rotation. Test images were made by rotating the unrotated standard image by angles ranging from −20° to +20° in 5° steps about the x-, y- and z-axes. A manual rotation tool within the spatial normalization software was used to perform the rotations and save images. The CH software was then used to reorient the test images to the unrotated standard image. The MSE between CHs of test and standard images was calculated before and after CH fitting for each test image.

Brain-Boundary Threshold (PET)

Partial-volume effects and blood flow in convex regions of the cortical surface are uniform in PET images, supporting the use of a single-threshold value for defining a brain boundary and for synthesizing its CH. A study of 12 ^{15}O-water and 8 ^{18}F-FDG images from subjects in MRI group 1 was performed to determine if an optimal threshold could be established. The MRI-derived CH for each subject was used as the target when performing a fit with the CH software. Test CHs were extracted from PET studies using thresholds defined as the percentage-of-maximum brain pixel values.

The quality of the fit was assessed using the residual root-mean-square (RMS) error of the distance from the target MR image to the test PET CHs for each subject after transformation. The goal was to find the threshold that gave the lowest average residual RMS error for all subjects. This was done by adjusting the threshold from 25% to 50% in increments of 5%. The CH software was configured to perform the fitting using five iterations with an option to exit if the MSE fell below 0.1. Default values for parameter convergence (0.05) and multiplier (20) were used (*24*). Testing was done with and without scaling to evaluate its effect on the residual RMS error. Thresholds were evaluated separately for the ^{18}F-FDG and ^{15}O-water images.

Spatial Normalization of Functional Images of Group 2

On the basis of the quality of CH global spatial normalization of MR images in groups 1 and 2 and PET-to-MRI fits observed during threshold testing, it was postulated that direct global spatial normalization of PET images (PET-to-template) could be achieved with similar accuracy and precision. The rationale was that the CH could be extracted in a highly consistent manner using a threshold-determined boundary, even for image types with lower spatial resolution, contrast and signal-to-noise ratio such as PET and SPECT. However, landmarks needed for testing spatial orientation of MRI to PET, such as the AC and PC, cannot be visualized in low-resolution PET images. Also, in this retrospective study, no fiducials (imbedded markers) were available for direct testing. To overcome these problems, the accuracy of the CH method for functional images was assessed using a three-pronged approach: (a) visual evaluation of PET-to-MRI matching, (b) measurement of fit quality using residual RMS values and (c) measurement of PET-to-MRI gray matter (GM) registration.

Visual Evaluation. Visual evaluation was done using paired MR and PET images from each subject. Each image was independently globally spatially normalized using the CH method. Bounding contours were extracted from PET images using 40% threshold values and overlaid onto the transformed MR image. The overlays were evaluated by looking for areas of match and mismatch between contours and the MR image. Additionally, the match

between PET-derived and template CHs was visually evaluated for each subject using the XSurfaceFit application (*24*).

Residual Root-Mean-Square Values. The high quality of fit of CH-transformed PET images seen during visual evaluation supports the use of residual RMS values as a measure of overall fit quality. Because MRI fit quality was already shown to be good (Tables 1 and 2), residual RMS values from PET were compared with those from MRI to determine how well they related. Nine PET images were analyzed for each of the 12 group 2 subjects, and mean residual RMS values were recorded. An analysis of covariance was done to test the covariance of mean residual RMS from PET with corresponding values from MRI in all 12 subjects.

PET-to-MRI Gray Matter Registration. It is well known that statistically significant extremum sites in PET functional activation studies develop from blood flow changes within GM (*12,13*). When identical PET and MR images are transformed in the same manner, PET-derived activation sites plotted onto MR images of the same subject should fall within the GM. Several tests were conducted to assess GM registration in paired PET/MR images. The chorus-minus-rest SPIs of 9 subjects from group 2 were used for this evaluation.

For each subject, positive extremum sites (increase in blood flow) with z scores > 2.30 were isolated and centroids calculated using intensity weighting in a 5 × 5 × 5 kernel (10 × 10 × 10 mm). Before centroid analysis, PET images were smoothed using a Gaussian filter to achieve a net FWHM of approximately 10 mm. This reduces the probability of more than one extremum within the search kernel. Extremum with fewer than two voxels within the kernel exceeding the threshold z score value were not used. The positional accuracy for centroid calculation was estimated to be approximately 1 mm (1/10 net FWHM) (*25*). Because of their high positional accuracy and constraint to GM, centroid-determined activation sites provide a unique landmark to test GM registration of PET and MR images of individual subjects.

Individual PET activation images (mean = 26 per subject) were recorded and plotted onto corresponding high-resolution MR images. The PET activation sites were well distributed throughout the cerebrum (37% temporal, 32% occipital, 11% frontal, 8%

TABLE 1
Talairach Atlas Brain Global Feature Measurements

Measurement	Method	x (mm)	y (mm)	z (mm)
Anterior commissure	SN	−0.3 ± 0.6	0.7 ± 0.8*	−0.2 ± 1.4
	CH1	−0.1 ± 1.2	−0.1 ± 1.4	−0.3 ± 1.4
	CH2	0.03 ± 0.1	−1.3 ± 1.5*	−0.4 ± 1.1
	CH pooled	−0.05 ± 0.9	−0.68 ± 1.6	−0.4 ± 1.2
Posterior commissure	SN	−0.3 ± 0.5*	−26.6 ± 1.5	1.2 ± 1.6*
	CH1	−0.1 ± 1.0	−26.8 ± 1.2	0.2 ± 1.4
	CH2	−0.04 ± 0.5	−27.2 ± 1.3	0.2 ± 1.5
	CH pooled	−0.1 ± 0.7	−27.0 ± 1.3	0.2 ± 1.4
Dimension errors	SN	−1.0 ± 1.4	−0.7 ± 1.5	−0.5 ± 1.1
	CH1	−1.3 ± 1.0*	−1.0 ± 2.4	−1.3 ± 3.6
	CH2	2.1 ± 2.2*	1.3 ± 2.1	−0.4 ± 2.8
	CH pooled	0.4 ± 2.4	0.2 ± 2.5	−0.9 ± 3.2

*Paired *t* test, *P* < 0.01.

SN = manual spatial normalization method; CH = convex-hull method; CH pooled = groups 1 and 2 combined.

Values are mean ± SD. SN and CH1 values are for group 1, and CH2 values are for group 2. n = 12 for both groups.

TABLE 2
Bounding-Box Coordinates in *Talairach Atlas* Space (in mm)

Landmark	CH1	CH2	CH pooled	Talairach
Left	−67.7 ± 1.3	−69.4 ± 1.2*	−68.6 ± 1.5	−68
Right	67.0 ± 1.8	68.6 ± 1.4	67.8 ± 1.8	68
Front	70.3 ± 2.4	70.3 ± 1.3*	70.3 ± 1.9*	69
Back	−100.7 ± 1.3*	103.1 ± 1.9	101.9 ± 2.0*	−103
Top	75.2 ± 2.6	74.2 ± 1.5	74.7 ± 2.1*	76
Bottom	−41.6 ± 2.4	−43.4 ± 2.3	42.5 ± 2.5	−42

*Paired *t* test, $P < 0.01$.

CH = convex-hull method; CH pooled = groups 1 and 2 combined.

Values are mean ± SD. CH1 values are for group 1, and CH2 values are for group 2. n = 12 for each group.

limbic, 7% parietal and 5% sublobar). Of these sites, 41% were on the left and 59% were on the right. The left–right distribution for the cerebellum was more balanced, with 48% on the left and 52% on the right. Each site was visually inspected and those falling within GM noted. Sites falling outside GM were labeled as either white matter (WM), cerebrospinal fluid (CSF) or other. The x, y and z distances to the nearest GM were estimated for WM- and CSF-labeled sites. Chance random spatial matching was evaluated using a set of uniformly distributed random coordinates constrained to the bounding limits of the 1988 *Talairach Atlas* brain (Table 2). These were scored as GM, WM or CSF for each MR image, and x, y and z distances to nearest GM were recorded as above. Points falling outside these tissues were not evaluated. For each subject, 50 random coordinates were used. Finally, extremum coordinates from the PET activation studies were randomly ordered and used to test GM matching in unmatched MR images. Each subject was evaluated with the number of random extremum coordinates equal to the number of true activation sites.

RESULTS

Spatial Normalization of Anatomic Images

All landmarks were measured relative to the designated origin (AC) at 128 mm from the left, 107 mm from the anterior and 88 mm from the superior image boundary.

Anterior Commissure Measurements. The means and SDs of the AC in millimeters after global spatial normalization are presented in Table 1. Accuracy of the manual spatial normalization method for the AC in group 1 subjects was slightly better than that reported in a previous evaluation (5). The AC error using the CH method for group 1 (template refinement group) is <1 mm. Paired *t* tests showed that the y coordinate for the AC was different from zero ($P < 0.01$) for manual spatial normalization (group 1) and CH (group 2) measurements. However, the absolute value of the distance was small (1.3 mm). The AC error using the CH method for pooled groups 1 and 2 was <1 mm for x, y and z coordinates. SDs were all <2 mm and similar between the spatial normalization method (using visual landmarks) and the CH method (surface based), although it was slightly larger for the CH method for the y coordinate.

Posterior Commissure Measurements. The means and SDs of the PC in millimeters after global spatial normalization are presented in Table 1. PC accuracy was assessed based on x and z coordinates that were both zero by definition. The y coordinate of the PC is not well established, although numerous values have been reported (7,11). The y coordinates of the PC compare well with the previously reported AC–PC distance (26.7 mm) measured in a different group of 16 normal subjects using the spatial normalization method (5). Paired *t* tests showed that x and z coordinates for the PC were both different from zero ($P < 0.01$) for the spatial normalization method. The +1.2-mm value of the z coordinate for the PC indicates a small mean angulation for the spatial normalization method relative to the CH method (~3° higher posteriorly). For the CH method, the mean y coordinate of the PC for group 2 was 0.4 mm posterior to that recorded for group 1. SDs were all <2 mm and similar for both the spatial normalization and CH methods.

Orientation. The mean AC–PC line orientation errors for groups 1 and 2 were <1.25° about the x-axis and <0.16° about the z-axis. Mean rotation of the midsagittal plane about the y- and z-axes was visually evaluated to be <1°. These measurements indicate that the mean orientation of the brain in MR images, CH spatially normalized using the refined template, conforms well to that defined in the *Talairach Atlas*.

Dimensional Errors. The x, y and z dimensions of spatially normalized brain images were compared with values previously reported for the 1988 *Talairach Atlas* brain (x = 136, y = 172 and z = 118 mm) (5). The dimensional errors in Table 1 are reported as measured-minus-*Atlas* values. The mean x, y and z dimensions for manual spatial normalization were within 1 mm of the atlas brain. The mean dimensional errors for the CH method in group 1 (template refinement) were all <1.3 mm, indicating the quality of the refinement of the template. The mean dimensional errors for the CH and spatial normalization methods were similar for group 1, all being slightly smaller than target values. The mean brain dimensions for the CH method in group 2 subjects were slightly larger than target values for x and y and slightly smaller for z. Pooled measurements resulted in mean x-, y- and z-dimensional errors of <1 mm. SDs of the dimensional errors for the CH method were consistently larger than those for the spatial normalization method. This was expected because the spatial normalization method used the same manual procedure to determine brain-bounding coordinates. Although paired *t* tests indicated real differences ($P < 0.01$) in the x dimensions for the CH method in groups 1 and 2, these differences were small in comparison with the dimension (1.5%).

Brain-Bounding Boxes. Statistics for *Talairach Atlas* coordinates of brain-bounding boxes measured on MR images spatially normalized using the CH method are presented in Table 2. Estimates of the bounding-box locations taken from the 1988 *Talairach Atlas* also are presented. Paired *t* tests showed several mean values to be different

from the Talairach values ($P < 0.01$). Mean values of measured bounding-box coordinates are within 1.4 mm for left and right dimensions, within 2.3 mm for front and back and within 1.3 mm for top and bottom boundaries. These results generally bracketed the *Talairach Atlas* values, with group 1 values being smaller and group 2 values being larger. Mean coordinates from pooled data resulted in values that were within 1.3 mm of the *Talairach Atlas* values for all six boundaries.

Transformation Parameter Reproducibility. The pooled SDs for rotation angles for the 81 PET images from 9 subjects were 1.28°, 0.84° and 0.45° for x-, y- and z-axis rotations, respectively. The ordering of these measurements follows the ordering of potential head rotations during scans. However, the larger x-axis rotation variance might also be due to the limited z-axis extent available for fitting. The reproducibility of z-axis rotations is believed to be least affected by head movement because the molded head restraint works well at restricting this type of movement, and the SD for this parameter possibly represents the reproducibility of motion-free studies of all three parameters. This is consistent with the maximum rotational error of <0.5° for the rotation study in 12 group 2 MR images.

The pooled SDs for translations were 1.19, 1.18 and 0.96 mm for the x-, y- and z-axis translations, respectively. These measurements indicate that variance in translation parameters is similar and small. As expected, these pooled SDs generally were smaller than the SDs for AC and PC landmarks in Table 1.

The pooled SDs for scaling were 0.007, 0.005 and 0.014 for x-, y-, and z-scale factors, respectively. The z-scale factor variance was largest, and this is believed to be due to the incomplete z-axis sampling of the brain (Figs. 3 and 4). Full brain images were not available for this repeat measurements study. The scale parameter variance estimates were assumed to be minimally affected by head movement because it is corrected during the fitting process.

CH fitting minimizes the distance between source and template surface models, and it is remarkable that internal landmarks, bounding limits and orientation are also well matched. Measurements from group 2 subjects, not used in template refinement, show that the CH method can accurately perform global spatial normalization to the 1988 *Talairach Atlas* standard using the refined template CH.

Template Fitting

Figure 3 is a typical example of the fit quality of the CH method for MR and PET images of the same subject. This subject was randomly selected from the MRI group used to refine the template (group 1). For all subjects in this group, the largest rotation angle for alignment was about the x-axis, with posterior regions rotated down. This rotation varied between modality, and for group 1 subjects it ranged from 2.7° to −6.5° for MR images and from −18° to −20° for PET images. Scale factors ranged from 1.02 to 1.10, with the largest scale factor seen for the z dimension. The overall quality of fit for group 1 subjects was excellent for all three image types, as indicated by small mean residual RMS errors and SDs (1.30 ± 4 mm for ^{15}O, 1.40 ± 0.21 mm for FDG and 1.49 ± 0.25 mm for MRI). Similar residual RMS values were seen for group 2. The small residual errors for fitting data from multiple subjects to a single template demonstrate the CH method's high intersubject consistency.

Rotational Characteristics

The MSEs between unrotated standard CHs and CHs rotated about the three major axes were measured. The mean and SEM of the MSE increased with increasing the angle for rotations about all axes (Fig. 5A). The MSE is the similarity measure minimized during the CH-fitting process, and the curves in Figure 5A measure the level of dissimilarity between standard *Talairach Atlas*-oriented and rotated CHs. The increasing MSE with increased angle is the result of asymmetry of the CH about the axis of rotation. MSEs were highest for rotations about the z-axis and lowest for rotations about the y-axis. This order is consistent with the visual impression of asymmetry of CHs in Figure 2. The residual MSEs between unrotated standard CHs and those reoriented using the CH method were also measured. Reorientation was excellent, with final orientation difference <0.5° in all cases. The residual MSE versus reorientation angle is plotted in Figure 5B. These data show that the residual MSE is approximately a linear function of the reorientation angle. Preprocessing was necessary to correct the nonzero MSE intercepts at 0° rotation in the raw data. The nonzero MSE intercept is characteristic of digital-image processing during rotation, resulting from trilinear interpolation and orientation-related sampling effects. Linear regression analysis was used to estimate the intercept for positive and negative angles for
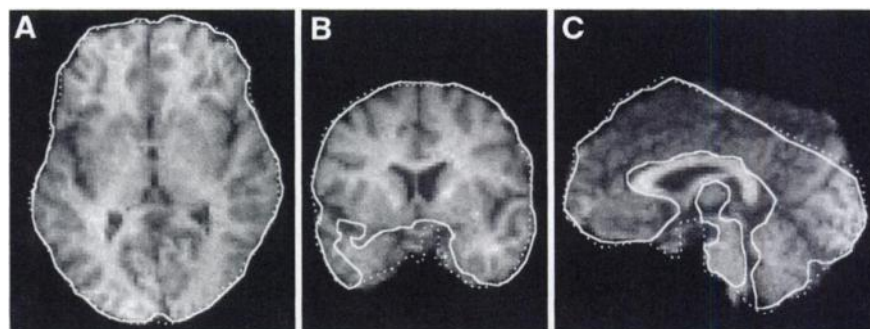

FIGURE 4. Overlays of ^{15}O-water (solid outline) and FDG PET (broken outline) brain contours onto axial (A), coronal (B) and sagittal (C) MR images from same subject after CH global spatial normalization. PET image contours were formed using 40% threshold. Highly concave portions of these contours are automatically excluded in development of CH (Fig. 3).
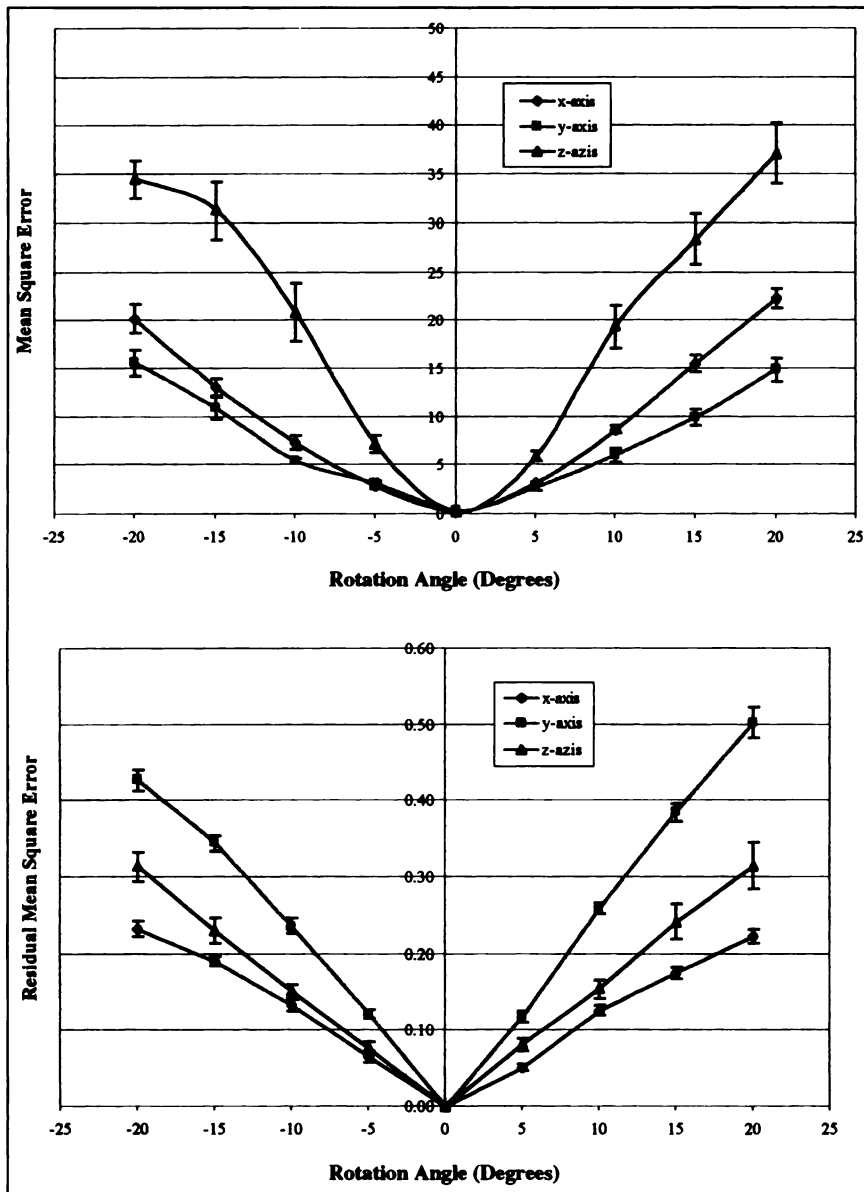
FIGURE 5. Mean and SEM values (error bars) for MSE between rotated and unrotated CHs (top) and residual MSE after reorientation of rotated CHs (bottom). Lines are for visual effect only. Head rotation for positive angles is nose down for x-axis, left side down for y-axis and nose left for z-axis rotations.

each curve and averaged. Corrected data for each curve were calculated by subtracting its estimated raw-data intercept from curve values. The corrected curve more closely represents the MSE characteristics due to physical effects of rotation and correctly reports a zero MSE at the 0° angle.

The residual MSE was <0.52 mm² (0.72-mm residual RMS value) for all reorientation angles and axes. The smallest residual MSE was for rotations about the x-axis and the largest for rotations about the y-axis at each angle. This is an ideal characteristic, because rotations normally encountered about the x-axis are large (up to 20°), with smaller rotations about the y- and z-axes. The rank order of residual MSE after CH fitting (y-z-x) is different from the order of the MSE due to the rotations (z-x-y) (Fig. 5). This is partly explained by the fact that MSEs after rotation are a measure of the CH's asymmetry, whereas residual MSEs are affected by CH asymmetry and the algorithm used in the fitting

process (*24*). These data indicate that the algorithm had more influence on residual MSE than CH asymmetry. Residual RMS values after reorientation are smaller than, but consistent with, residual RMS values measured for threshold testing (Fig. 6). Smaller values were expected since that analysis was done using images from different imaging modalities.

Brain-Boundary Threshold (PET)

Graphs of average residual RMS error versus threshold for the 12 group 1 subjects are presented in Figure 6. Residual RMS error is calculated as the square root of the residual MSE reported by the surface-fitting software (*24*). It is a measure of the mean distance in millimeters from template to test CHs measured along a line from the centroid of the template CH. The average residual RMS error trend was modeled as a quadratic function using the polynomial
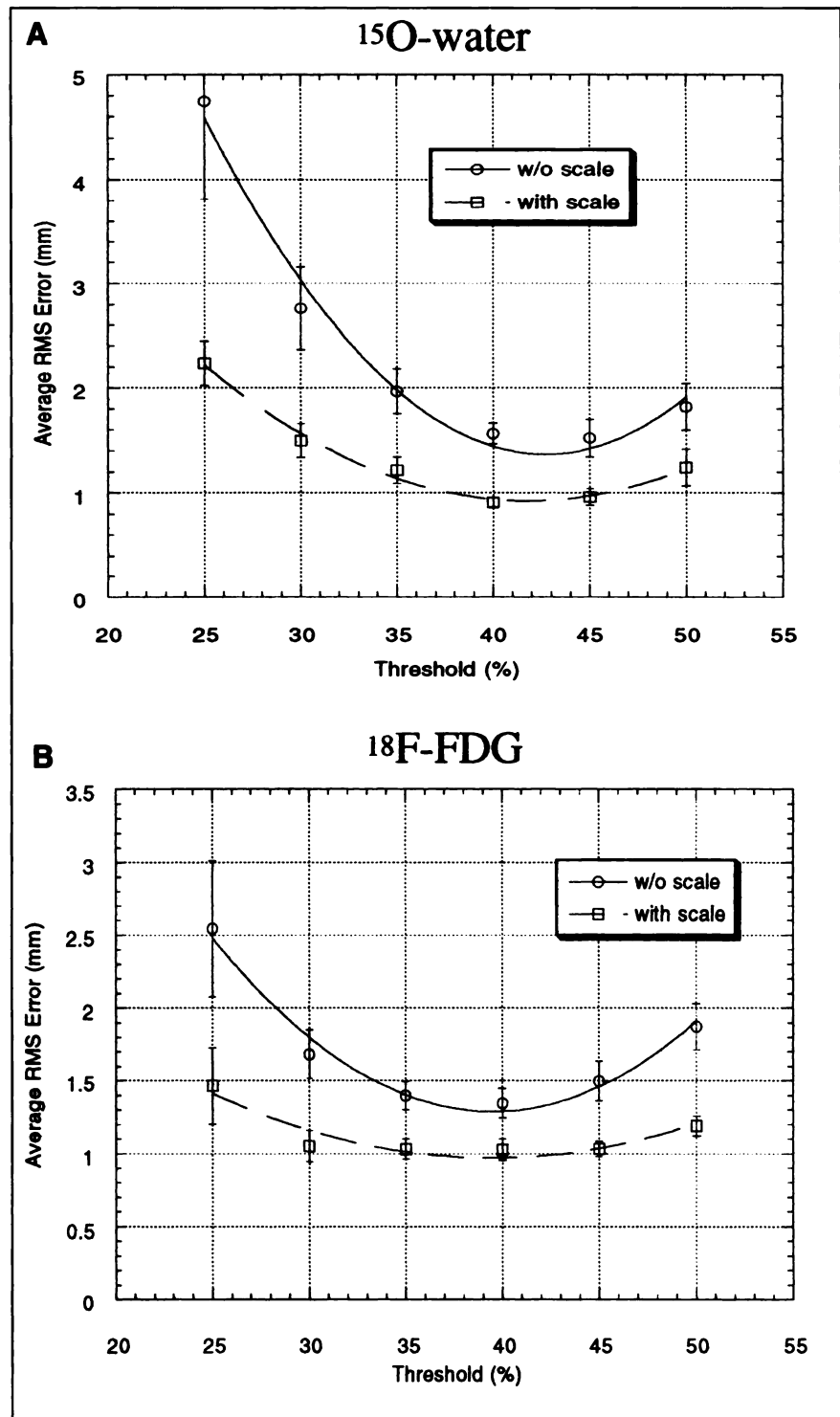
FIGURE 6. Average residual RMS error curves have minimum near 40% threshold for both ¹⁵O-water (A) and FDG PET images (B). SDs (error bars) follow this same trend. w/o = without.

fitting procedure provided by KaleidaGraph 3.0 0.1 (Abel-beck Software, Synergy Systems, Reading, PA) and the results plotted in Figure 6. The correlation values for this fit were >0.99 for ¹⁵O-water data and >0.94 for ¹⁸F-FDG data. The minimum of each curve was calculated as the point with zero slope from the model quadratic equations. For ¹⁵O-water data, this resulted in thresholds of 42.7% without scaling and 41.7% with scaling. For ¹⁸F-FDG data, the

minimum residual error occurred at thresholds of 39.5% without scaling and 39.4% with scaling. For both ¹⁵O-water and ¹⁸F-FDG data, the average residual RMS error was smaller with scaling (~1 mm) than without (~1.5 mm). This may be due to slight differences in the spatial calibration of the PET and MR imagers that are compensated by scaling. One recommendation to correct for spatial calibration differences in cross-modality registration is to perform the

analysis with scaling (22,26). The average minimum-error threshold for both image types was 40.6% with scaling and 41.1% without scaling. The SD of the residual RMS error was evaluated in a similar manner, and the resulting minimum variance threshold value was also approximately 41%.

On the basis of these results and the fact that the error-versus-threshold curves are fairly broad near their minimum, a practical operating threshold of 40% was selected for both ^{15}O-water and ^{18}F-FDG when creating CHs. The convex nature of the brain boundary, defined in a PET image using this threshold, is optimally matched with that defined by an MR image. Because of this match, the 40% threshold was also considered optimal for direct fitting of PET images to the CH template (i.e., for global spatial normalization). The small residual errors for fitting PET CHs to MRI CHs in the same subject (Fig. 6) demonstrate the intermodality consistency of the CH method.

Spatial Normalization of Functional Images

Visual Evaluation. Brain-bounding contours extracted from ^{15}O-water and FDG PET images overlaid onto the MR image of the same subject illustrate several important features of the CH method (Fig. 4). MR and PET images were independently spatially normalized and resliced to 2-mm isometric voxels. First, as seen in the coronal and sagittal sections, the contours indicating the 40% boundary for PET images can be highly concave. However, concave regions are replaced by convex estimates during CH synthesis. Second, the limited z-axis extent of the PET imager is demonstrated in the sagittal image. Third, as seen in the sagittal PET image (Fig. 4C), contours of several deeper structures (corpus callosum, caudate and brain stem) follow their anatomic outlines in the MR image. Finally, there is good correspondence between the ^{15}O-water and FDG PET contours and the MR image for convex boundary regions. Fitted CHs were viewed using XSurfaceFit from opposite sides of the x-, y- and z axes for each PET subject evaluated (12 from group 1 and 9 from group 2). All subject-derived CHs were judged to conform well to the template CH and were similar to those illustrated in Figure 3.

Residual Root-Mean-Square Values. The means and SDs of residual RMS values for the CH method in the 12 group 2 subjects were 1.47 ± 0.17 mm for ^{15}O-water PET images and 1.36 ± 0.18 mm for MR images. These mean residual RMS values were slightly larger than the approximately 1-mm value measured when PET images were fitted directly to MR images for the same subject (Fig. 6) but similar to those for group 1. The small SDs for residual RMS errors for both PET and MRI demonstrate the similarity of brain CHs to the template within this group. Analysis of variance between PET and MRI residual RMS values revealed a highly significant F value ($P < 0.003$), and correlation analysis yielded an adjusted R value of 0.77. These results, coupled with visual evaluations, indicate that PET and MR images are fitted to the template CH with similar accuracy.

PET-to-MRI Gray Matter Registration. Three sets of coordinate data were tested on images of 9 group 2 subjects after CH global spatial normalization. Points outside GM were labeled as WM, CSF or other. The *other* category included brain stem and vessels and was <3% of all labeled points. Therefore, only GM, WM and CSF sites were evaluated further. For uniformly randomized *Talairach Atlas* coordinate data, the fraction of sites falling in GM (38.3%) and WM (37.4%) are similar and approximately 50% larger than the CSF fraction (24.3%). Randomized coordinates outside the brain were not included. For individual PET activation coordinate data, the GM fraction rose to 63.8%, WM dropped to 26.3% and CSF dropped to 10.0%. For PET activation coordinates randomized across subjects, intermediate fractions were seen (GM = 43.2%, WM = 33.6% and CSF = 23.1%).

Although individual subject results did not produce a 100% GM fraction, they did indicate significant overlap of PET activation sites with GM. Additionally, many of the WM and CSF sites were very near GM. A cumulative histogram was calculated to quantify this observation. It showed increases in the percentage of GM sites when non-GM sites at various distances from the original GM boundary were included (Fig. 7). Boxcar distance (sum of x, y and z distances in millimeters) was used to standardize bins for the histogram. This distance measure naturally combines sense and axis differences into a single measure, and boxcar-type manipulations were used to determine the shortest distance between non-GM sites and GM. Boxcar distance tends to overestimate Euclidean distance slightly, but it provides similar results, as was verified for group 2. Figure 7 shows that individual PET activation sites provide the largest GM fraction at each boxcar distance. The GM fraction approached 90% at a boxcar distance of 2 mm (mean distance = 1.59 mm). The GM fractions for random PET activations increased rapidly and were similar to
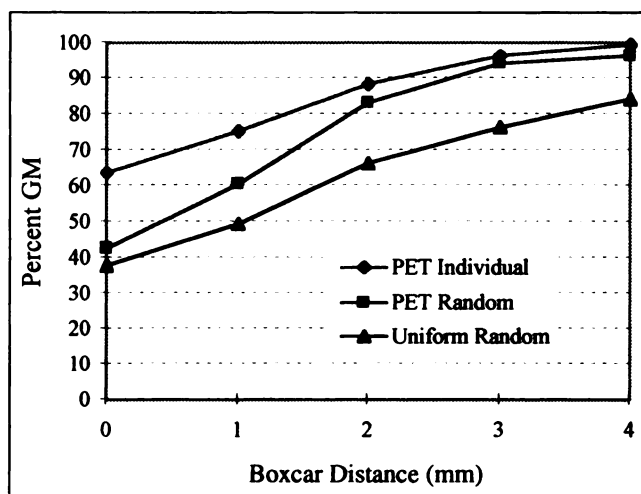

FIGURE 7. Cumulative histogram of percentage of GM versus boxcar distance for individual PET activation sites, randomized PET activation sites and sites uniformly distributed within *Talairach Atlas* brain.

individual PET activation fractions (both >95%) for boxcar distances of 3 mm or more. The mean absolute distance for a boxcar distance of 3 mm in the individual PET activation data was 2.40 mm. Uniform random sites resulted in GM fractions that increased linearly but were consistently lower for all distances. Sites with boxcar distances of 5 mm were grouped into a single category (0.5% for individual PET activations, 3.5% for randomized PET activations and 16% for uniformly randomized sites). For the uniformly randomized sites, most distances in this category were much larger than 5 mm, whereas for PET activation sites most were near 5 mm.

Complete PET-to-MRI GM registration is unreasonable considering that GM, especially cortical GM, may differ geometrically because of differences in head orientation and physiological factors during PET and MRI and regional distortions in MR images. When combined with confirmatory results for visual and residual RMS evaluations, the high GM fractions for individual PET activation sites (Fig. 7) demonstrate a high level of PET-to-MRI GM registration. As demonstrated using randomized PET activation coordinates, PET-to-MRI GM matching also is good when sites from one subject are plotted onto another, as is common with atlas referencing. These tests show that functional global spatial normalization can be performed very well without the aid of an MR image.

DISCUSSION

These results show that anatomic (MRI) and functional (PET) images globally spatially normalized using the CH method conform well to global brain features of the *Talairach Atlas*. The small differences at the extreme bounds likely reflect differences between the *Talairach Atlas* and the brains in the two subject groups in this study. Spatial precision of these features generally was good (SDs of 2 mm or less) and similar for deep and surface landmarks. For studies in which four or more images are averaged, this should be <1 mm. This low level of global-feature spatial variability should prove useful for averaged paired subtractions in functional imaging studies. Landmark conformance is good (AC, PC and bounds), and the overall quality of the fit for all 24 MR images to the template was exceptional, as indicated by the low group average residual RMS error of 1.43 mm (SD = 0.22 mm, maximum = 1.90 mm). It should be emphasized that although mean locations of tested sites conformed well to the *Talairach Atlas*, individual locations can be several millimeters from corresponding *Atlas* sites, as indicated by the SDs in Tables 1 and 2.

Convex-Hull Synthesis

For template and subject CHs tested to date, the CH algorithm has provided highly convex representations across the brain surface (Fig. 2). The greatest challenge in synthesizing the CH is the inferior brain surface, where there are large concave regions and slight residual concavity can be seen (Fig. 2). As implemented, the CH algorithm correctly extracts portions of the inferior surfaces of the temporal lobe and cerebellum and yields a consistent and highly convex surface over the remainder of the inferior hull. The slight concave regions seen along the inferior margin have not caused any fitting problems. As synthesized, the CHs have proven to be well suited for use as surface models for global spatial normalization. A fast, three-dimensional algorithm such as Quickhull (27) was not considered important since processing speed and quality of the head model were both acceptable. Processing time for PET images (128 × 128 × 25 matrix, 16-bit data) was 20 s on a Sun Sparcstation 20 (Sun Microsystems). This increased to 4 min 45 s for MR images (256 × 256 × 128 matrix, 16-bit data). For MR images, approximately half of the processing time was for data input and CH extraction and half was for surface fitting. The largest component of total processing time for MR images was for manual editing to remove nonbrain surfaces, which can take several hours to do well.

Automated CH synthesis removes operator bias and eliminates the operator training needed to accurately define landmarks. The template CH covers the entire brain, including the cerebellum (Fig. 2). It was developed using high-resolution MR image data and therefore has a large number of surface points (4420 points in 100 contours). Subject CHs are extracted in a point-data format. CHs for MR images consisted of 4000–5000 surface points. CHs for PET images had approximately 400 surface points (average of 415 for ^{18}F-FDG and 429 for ^{15}O-water studies in group 1). This smaller number of points was due to the limited z-axis extent and lower spatial resolution of the PET imager. The number of points used is 3–4 times that reported by Pelizzari et al. (21) as acceptable for registering CT, PET and MR images. The smaller number of points in PET CHs did not adversely affect mean residual RMS errors of PET (1.40 ± 0.22 mm) compared with MRI (1.43 ± 0.22) on the basis of pooled results (n = 24) of groups 1 and 2.

Brain Boundary by Thresholding

Thresholding in PET images to isolate the brain from nonbrain regions is a common practice in functional image analysis (12,13). Although the optimal threshold can vary because of differences in factors such as tomographic reconstruction and postprocessing filters, the 40% value is believed to be a reasonable compromise for PET studies in healthy subjects. Should a threshold-determined boundary contain concave regions, they will be eliminated during the CH-synthesis process (Figs. 3 and 4). Although the 40% threshold was optimal for the PET images used in this study, this value might be different for other radionuclides and imaging modalities. If a single threshold is to be used to determine the brain boundary, it is recommended that the threshold that minimizes the difference between CHs of MR and the test brain images be determined, as was done in this study.

Suprathreshold pixel values that fall outside the brain must be avoided. One such problem for CBF PET studies is scalp activity when blood flow to the skin is high. The use of

right-side markers with high specific activity will also cause this problem. Additionally, other parts of the body within the FOV may exceed the threshold value. In each case, the problem can be resolved by preprocessing to remove unwanted regional activity. Alternative methods that can accurately extract brain surfaces and remove nonbrain regions can be used for preprocessing to derive an appropriate boundary for CH spatial normalization.

On MR and CT images, the pixel values for structures outside the brain are too high to use a single threshold for brain-boundary detection. The CH method requires preprocessing of such images to remove nonbrain tissues. It also is important to remove the brain stem if it extends below the inferior limit of the cerebellum. Use of an automated method to remove nonbrain tissues (28) was not investigated, but such processing might provide a time-efficient processing stream for MR and CT images.

Limited Field of View

The PET scanner used in this study (GE/Scanditronix 4096) has a limited z-axis FOV (15 slices at 6.5-mm spacing). This z-FOV is not sufficient to image the full extent of the brain (Figs. 3 and 4). The SurfaceFit algorithm (21,23) works well in this case by performing a best fit of the subject's CH (partial head) to the template CH (full head). Limited-FOV PET images generally include either the temporal lobe or the top of the brain, but not both. Measured residual RMS errors were similar in both cases, and all were less than the 2-mm value established for rejection. It is believed that the CH method will perform well with newer PET imagers with extended z-axis FOV and SPECT imagers that can image the entire brain.

SPECT Applicability

The single-threshold approach to global spatial normalization using the CH method should extend to SPECT brain procedures using labeled tracers such as ^{99m}Tc-hexamethyl propyleneamine oxime (29) or ^{99m}Tc-ethyl cysteinate dimer (ECD) (30) when brain-surface values are larger than surrounding nonbrain values. Minoshima et al. (8) developed an improved method for spatial normalization of PET images, and Bartenstein et al. (31) used this method with regional CBF SPECT images in a study of Alzheimer's disease. Schiepers et al. (32) used a different method for spatial normalization in a study of normal brain perfusion patterns of ^{99m}Tc-ECD in children. These studies indicate a trend in SPECT brain imaging toward the use of spatial normalization for averaging across groups of subjects to define effects. The CH software and template provide a means to rapidly perform this spatial normalization using an automated and validated method. In preliminary testing of the CH method with SPECT, images appeared to be transformed correctly, with residual errors similar to those found with MRI and PET.

Regional Image Distortions

Regional spatial distortions of the imaging system can alter the accuracy of boundary extraction and affect the quality of global spatial normalization. Inherent spatial distortions of PET and SPECT imagers often are ignored because they usually are small compared with the spatial resolution (21,22,26,33). Most modern SPECT cameras use spatial linearity corrections to remove minor regional spatial distortions. Although regional geometric distortions in MR images have been shown to effect registration accuracy (34), Hemler et al. (35) reported that they have little effect on surface-based registration. The low residual errors (1–1.5 mm RMS) for fitting PET and MR images from healthy subjects to the template CH suggest that regional distortions, if present, are not a major factor in the quality of CH global spatial normalization.

Regional Brain Distortions

Because the design of this study was to evaluate the CH method in healthy subjects, regional spatial distortions of the brain due to anatomic and/or functional lesions were not evaluated. However, the greatest effect is anticipated for lesions on or near convex brain surfaces. The majority of the cortical surface falls within concave regions, and the CH guards against small regional changes there. CH global spatial normalization has been used in over 100 brains, and activations have not caused apparent fitting problems. Should regional changes cause the maximum brain value to change, this may affect the accuracy of boundary detection. However, as shown in Figure 6, small changes have little effect on fit quality. If a lesion alters a convex surface it may or may not appreciably affect the quality of CH global spatial normalization. The CH method is based on error minimization over the entire CH surface, and this helps moderate adverse effects of small perturbations. If spatial normalization is problematic, it likely will be reflected by significant changes in the residual error. For the PET and MR brain images analyzed in this study, a residual RMS error > 2 mm was used to indicate poor fit. This value is 2.5 SDs above the mean residual RMS error determined for MRI and PET in the group 1 subjects. In future versions of the CH software, outlier surface points may be ignored during the final fit to compensate for small regional brain distortions (lesions); however, this strategy has not yet been tested.

Global Versus Regional Spatial Normalization

Numerous interactive, landmark-based methods have been reported for global spatial normalization of PET images (1,2,5,36). Although regional spatial normalization can provide better spatial matching of more and smaller anatomic features, little evidence has been presented to show that this improves spatial matching of functional centers in the brain (4,10). One use of a nonlinear warping method for regional spatial normalization was reported to have little effect on location of peak activation sites in ^{15}O-water PET (36). One study of regional spatial normalization methods indicated that nearly 90% of the difference between MR brain images is resolved with a nine-parameter global affine transformation (4). Regional spatial normalization, based on

current high-resolution MRI, may not be the solution, because microstructure may not follow macrostructure in numerous locations within the brain (37,38). It remains to be shown whether reducing anatomic variability beyond that provided by the CH method will greatly reduce functional variability, especially when reporting group effects in a standard atlas space.

Talairach Atlas Coordinates

CH global spatial normalization provides a means to rapidly transform a brain image to Talairach space in which coordinates can be used to indirectly reference locations of interest. Using Talairach coordinates, names for brain locations can be retrieved from the automated brain-label database server, the Talairach Daemon (39). It is Internet accessible and provides data in the form of brain labels and structure probabilities indexed by Talairach Atlas coordinates (http://ric.uthscsa.edu, Projects). The Talairach labels database contains anatomic labels for the 1988 Talairach Atlas brain (39). The Talairach Daemon was used to calculate the percentage of PET activation sites by lobe for the PET-to-MRI GM registration study. A structure probability maps database is also provided by the Talairach Daemon server. It gives the probability of occurrence for several brain structures indexed by coordinate. This database was derived from automatically segmented brain structures in healthy subjects (10). The structures from each subject were transformed to the 305 Brain Atlas (16,40) in which percentage of structure overlap was converted to a probability. The structure probability maps are referenced to a globally transformed brain image space and are well suited for use after CH global spatial normalization.

Scope of Use

Global spatial normalization satisfies the processing needs for most functional brain imaging studies and can be quickly and reproducibly accomplished by the CH method. CH global spatial normalization was designed for use with anatomic (MRI, CT) and functional (PET, SPECT) tomographic images. Spatially normalized functional PET images register well with spatially normalized anatomic MR images (Figs. 1, 3, 4 and 7), supporting fusion for display of findings. The CH method was not evaluated for functional MRI (fMRI), but preliminary tests indicate that it will work well with echo-planar fMRI. It was not evaluated with CT or SPECT, but preliminary testing with SPECT images produced similar results. Although it has not been evaluated for clinical applications, CH global spatial normalization should prove useful in clinical as well as research settings. The processing is fast, supporting easy integration into a busy clinical setting.

CONCLUSION

The CH, a surface model of the human brain, was shown to be highly consistent across subjects and imaging modalities. A highly consistent relationship between the brain's CH and the mean location of two deep landmarks (AC and PC)

was found. This was also seen for brain bounding-box dimensions and locations. The variance for surface and interior landmarks was similar. The accuracy of CH global spatial normalization for PET functional images was shown to be similar to that for MR images. The registration of PET activation sites with GM in independently spatially normalized MR images was shown to be good. These findings indicate that the global spatial normalization provided by the CH method is well suited for the preprocessing required in the development of SPIs used in the formal statistical analysis of functional brain studies.

REFERENCES

1. Fox PT, Perlmutter JS, Raichle ME. A stereotactic method of anatomical localization for positron emission tomography. J Comput Assist Tomogr. 1995;9:141–153.
2. Friston KJ, Passingham RE, Nutt JG, Heather JD, Sawle GV, Frackowiak RSJ. Localization of PET images: direct fitting of the intercommissural (AC-PC) line. J Cereb Blood Flow Metab. 1989;9:690–695.
3. Steinmetz H, Furst G, Freund HJ. Cerebral cortical localization: application and validation of the proportional grid system in MR imaging. J Comput Assist Tomogr. 1989;13:10–19.
4. Collins DL, Neelin P, Peters TM, Evans AC. Automatic 3D intersubject registration of MR volumetric data in standardized Talairach space. J Comput Assist Tomogr. 1994;18:192–205.
5. Lancaster JL, Glass TG, Lankipalli BR, Downs H, Mayberg H, Fox PT. A modality-independent approach to spatial normalization. Hum Brain Mapp. 1995;3:209–223.
6. Downs JH, Lancaster JL, Fox PT. 3-D surface based spatial normalization using a convex hull. In: Thatcher R, Zeffiro T, Huerta M, eds. Advances in Functional Neuroimaging: Technical Foundations. Orlando, FL: Academic Press; 1994:131–136.
7. Downs JH. A Convex Hull Method for Surface-Based Spatial Normalization of the Brain [dissertation no. 9517506]. Ann Arbor, Mich: UMI Dissertation Services; 1994.
8. Minoshima S, Koeppe RA, Mintum MA, et al. Automated detection of the intercommissural line for stereotaxic localization of functional brain images. J Nucl Med. 1993;34:322–329.
9. Friston KJ, Ashburner J, Frith CD, Poline JB, Heather JD, Frakowiak RSJ. Spatial registration and normalization of images. Hum Brain Mapp. 1995;3:165–189.
10. Collins DL, Holmes CJ, Peters TM, Evans AC. Automatic 3D model-based neuroanatomical segmentation. Hum Brain Mapp. 1995;3:190–208.
11. Talairach J, Tournoux P. Co-Planar Stereotaxic Atlas of the Human Brain. New York, NY: Thieme Medical Publishers; 1988.
12. Fox PT, Mintum MA, Reiman EM, Raichle ME. Enhanced detection of focal brain responses using intersubject averaging and change distribution analysis of subtracted PET images. J Cereb Blood Flow Metab. 1988;8:642–653.
13. Friston KJ, Frith CD, Liddle PF, Frakowiak RSJ. Comparing functional (PET) images: the assessment of significant change. J Cereb Blood Flow Metab. 1991;11:690–699.
14. Fox PT. Spatial normalization: origins, objectives, applications and alternatives. Hum Brain Mapp. 1995;3:161–164.
15. Fox PT, Mikiten S, Davis G, Lancaster JL. BrainMap: a database of human functional brain mapping. In: Thatcher RW, Zeffiro T, Huerta M, eds. Advances in

Functional Neuroimaging: Technical Foundations. Orlando, FL: Academic Press; 1994:95–106.

16. Mazziotta JC, Toga AW, Evans A, Lancaster JL, Fox PT. A probabilistic atlas of the human brain: theory and rational for its development. *Neuroimage*. 1995;2:89–101.

17. Bloch I. *3-D Pattern Recognition, Application to Chemical Molecule* [PhD thesis no. 90E018]. Paris, France: Telecom; 1990.

18. Mangin JF, Frouin V, Bloch I, Bendriem B, Lopez-Krahe J. Fast nonsupervised 3D registration of PET and MR images of the brain. *J Cereb Blood Flow Metab*. 1994;14:749–762.

19. Gonzalez RC, Woods RE. *Digital Image Processing*. Reading, MA: Addison-Wesley; 1992.

20. Ono M, Kubik S, Abernathey CD. *Atlas of the Cerebral Sulci*. New York, NY: Theime Medical Publishers; 1990.

21. Pelizzari CA, Chen GTY, Spelbring DR, Weichselbaum RR, Chen CT. Accurate three-dimensional registration of CT, PET, and/or MRI images of the brain. *J Comput Assist Tomogr*. 1989;13:20–26.

22. Turkington TG, Jaszczak RJ, Pelizzari CA, et al. Accuracy of registration of PET, SPECT and MR images of a brain phantom. *J Nucl Med*. 1995;34:1587–1594.

23. Melkman AA. On-line construction of the convex hull of a simple polyline. *Informatics Processing Lett*. 1987;25:11–12.

24. Pelizzari CA. Installation and User's Guide for University of Chicago Image Registration Software (SurfaceFit). Available at: http://www.radonc.uchicago.edu/~chuck/imagcorr. Accessed April 23, 1999.

25. Mintum MA, Fox PT, Raichle ME. A highly accurate method of localizing regions of neuronal activation in the human brain with positron emission tomography. *J Cereb Blood Flow Metab*. 1989;9:96–103.

26. Strother SC, Anderson JR, Xu XL, Liow JS, Bonar DC, Rottenberg DA. Quantitative comparisons of image registration techniques based on high-resolution MRI of the brain. *J Comput Assist Tomogr*. 1994;18:954–962.

27. Barber CB, Dobkin DP, Huhdanpaa HT. The Quickhull algorithm for convex hulls. *ACM Trans Math Software*. 1996;22:469–483.

28. Ardekani BA, Braun M, Kanno I, Hutton BF. Automatic detection of intradural spaces in MR images. *J Comput Assist Tomogr*. 1994;18:963–969.

29. Neirinckx RD, Canning LR, Piper IM, et al. Technetium-99m d,l-HM-PAO: a new radiopharmaceutical for SPECT imaging of regional cerebral blood perfusion. *J Nucl Med*. 1987;28:191–202.

30. Vallabhajosula S, Zimmerman RE, Picard M, et al. Technetium-99m-ECD: a new brain imaging agent: in vivo kinetics and biodistribution studies in normal human subjects. *J Nucl Med*. 1989;30:599–604.

31. Bartenstein P, Minoshima S, Hirsch C, et al. Quantitative assessment of cerebral blood flow in patients with Alzheimer's disease by SPECT. *J Nucl Med*. 1997;38:1095–1101.

32. Schiepers C, Verbruggen A, Caesar P, De Roo M. Normal brain perfusion pattern of technetium-99m-ethyl cysteinate dimer in children. *J Nucl Med*. 1997;38:1115–1120.

33. Woods RP, Cherry SR, Mazziotta JC. Rapid automated algorithm for aligning and reslicing PET images. *J Comput Assist Tomogr*. 1992;16:620–633.

34. Maurer CR, Aboutanos GB, Dawant BM, et al. Effect of geometrical distortion correction in MR on image registration accuracy. *J Comput Assist Tomogr*. 1996;20:666–679.

35. Hemler PF, Van den Elsen PA, Sumanaweera TS, Napel S, Dance J, Adler JR. A quantitative comparison of residual error for three different multimodality registration techniques. In: Bizais Y, Barillot C, Di Paola R, eds. *Information Processing in Medical Imaging 1995*. Dordrecht, The Netherlands: Kluwer Academic; 1995:251–262.

36. Minoshima S, Koeppe RA, Kirk AF, Kuhl DE. Anatomic standardization: linear scaling and nonlinear warping of functional brain images. *J Nucl Med*. 1994;35:1528–1537.

37. Zilles K, Schleicher A, Langemann C, et al. Quantitative analysis of sulci in the human cerebral cortex: development, regional heterogeneity, gender difference, asymmetry, intersubject variability and cortical architecture. *Hum Brain Mapp*. 1997;5:218–221.

38. Roland PE, Geyer S, Amunts K, et al. Cytoarchitectural maps of the human brain in standard anatomical space. *Hum Brain Mapp*. 1997;5:222–227.

39. Lancaster JL, Rainey LH, Summerlin JL, et al. Automated labeling of the human brain: a preliminary report on the development and evaluation of a forward transform method. *Hum Brain Mapp*. 1997;5:1–5.

40. Evans AC, Collins DL, Mills SR, Brown ED, Kelly RL, Peters TM. 3D statistical neuroanatomical models from 305 MRI volumes. In: *Proceedings of the IEEE-Nuclear Science Symposium and Medical Imaging Conference*. Piscataway, NJ: IEEE Inc., 1993:1813–1817.